An MPC-based Energy Management System for a Hybrid Electric Vehicle

Alessandro Serpi, Mario Porru

Department of Electrical and Electronic Engineering
University of Cagliari
Cagliari, Italy
alessandro.serpi@unica.it

Novel Electric Propulsion Systems
NEPSY srl
Cagliari, Italy
info@nepsy.it

***Abstract*—A real-time Energy Management System (EMS) is presented in this paper, which aims at minimizing the operating costs of a Hybrid Electric Vehicle (HEV) equipped with different energy storage units (fuel cell, supercapacitors, batteries). The proposed EMS manages all HEV operating constraints properly through a Model Predictive Control (MPC) approach, which identifies the allowable ranges of each variable based on system modelling and actual HEV operating conditions. The optimization is then carried out by means of suitable look-up tables, which are accessed in accordance with the variable ranges previously computed. The effectiveness of the proposed MPC-based EMS is verified through numerical simulations, which also regard a rule-based EMS for comparison purposes.**

Keywords—Batteries, Cost function, Electric vehicle, Energy management, Fuel cells, Optimization, Predictive control, Supercapacitors

I. INTRODUCTION

The Energy Management System (EMS) covers a fundamental role in Hybrid Electric Vehicles (HEVs), especially when several energy sources are concerned [1], [2]. The EMS main task is satisfying the HEV power demand at any operating condition, by sharing it among the different energy sources onboard in accordance with their inherent features and actual capabilities (dynamic response, operating constraints, energy content, etc.).

Different approaches can be followed in designing an EMS for HEVs, each of which presents inherent advantages and drawbacks. Frequency-based approaches split the required power demand in accordance with its harmonic content by means of appropriate low- or high-pass filters [3], [4]: low-frequency power components are generally handled by low-dynamic energy storage units, such as Fuel Cells (FCs) and Battery Packs (BPs), while high-frequency power components are managed mostly by Supercapacitors (SCs) or flywheel energy storage systems, which are characterized by much faster dynamic response and cycling capability. Frequency-based EMSs achieve fair performance and are simple to implement but suffer from unoptimized HEV operating costs and constraints management. Better performance is foreseen by rule-based approaches, which split the HEV power demand in accordance with a set of rules [5], [6]; these are generally defined offline based on system constraints and desired performance, but they could be adapted also online in order to improve HEV operation further. Alternatively, optimization-based methods can be employed, which rely on advanced but generally complex control algorithms that ensure HEV performance optimization at different operating conditions [7]–[11].

Optimisation-based EMSs can be further classified in global and real-time approaches: the former requires prior information on the expected power demand over a given time horizon [7], [8], while the latter minimises a given cost function based on instantaneous parameter and/or operating conditions only [9]–[11]. Global approaches generally perform better than real-time methods, thus they represent the best solutions for smart grid applications that benefit from power scheduling and load forecasting. On the other hand, real-time EMSs are much more feasible to implement when vehicular applications are concerned, by turning a global optimisation problem into an instantaneous minimisation task [10], [11].

In this context, a real-time EMS is presented in this paper, which is developed within the competition promoted in [12] at the aim of minimising the operating cost of a HEV equipped with FC, SC and BP. In particular, a Model Predictive Control (MPC) approach is applied in order to manage all HEV operating constraints appropriately. Furthermore, suitable Look-Up Tables (LUTs) have been defined and managed in real-time in order to select the most suitable reference signals that comply with all system constraints at any operating conditions. The effectiveness of the proposed MPC-based EMS is verified through numerical simulations, which also regard a basic rule-based EMS for comparison purposes.

II. HEV OVERVIEW AND MODELLING

The schematic overview of the Electric Propulsion System (EPS) of the HEV considered in this paper is shown in Fig. 1. Particularly, starting from the top-left branch and rotating in counter-clockwise direction, the EPS consists mainly of:

- a Fuel Cell (FC), which is coupled to the DC-link through a DC-DC converter and an inductive filter;
- a Supercapacitor module (SC), which is coupled to the DC-link similarly to FC;
- an electric motor and its auxiliaries, which constitute the Electrical Drive (ED) of the HEV;
- a Battery Pack (BP), which is directly connected to the DC-link;
- a Brake Resistor (BK), which enables rheostatic braking as needed.

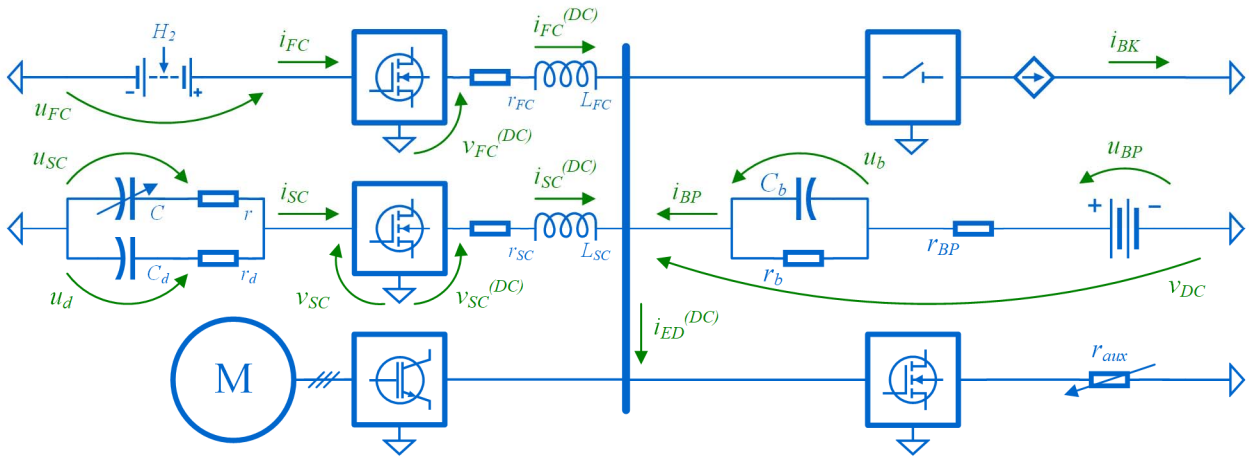

Fig. 1. Schematic overview of the HEV electric propulsion system considered in this paper: FC, SC, ED, BP and BK branches.

Modelling of each EPS component, which is derived from the files provided within the competition promoted in [12], is detailed in the following subsections because it is preparatory for developing the MPC-based EMS proposed in this paper.

A. Fuel Cell

The FC is modelled by its polarization curve and by the relationship between H_2 consumption and FC current, which are expressed respectively as

$$v_{FC} = \sum_{k=0}^{3} a_k \, i_{FC}^k \,, \quad \frac{d\,m_{H_2}}{dt} = \sum_{k=0}^{1} b_k \, i_{FC}^k \quad (i_{FC} > 0) \tag{1}$$

in which v_{FC} and i_{FC} denote FC voltage and current, while a_k and b_k are appropriate numerical coefficients [13], [14]. Instead, an ideal model is considered for the DC-DC converter, namely the following relationship holds:

$$p_{FC} = v_{FC}\, i_{FC} = v_{FC}^{(DC)}\, i_{FC}^{(DC)} \,, \quad v_{FC}^{(DC)} = m_{FC} v_{FC} \tag{2}$$

in which p_{FC} is the FC power, the superscript $^{(DC)}$ denotes voltage and current values at the DC-link side, while m_{FC} is the voltage conversion ratio. Considering the inductive filter, the following relationship applies:

$$v_{FC}^{(DC)} = r_{FC}\, i_{FC}^{(DC)} + L_{FC} \frac{d i_{FC}^{(DC)}}{dt} + v_{DC} \tag{3}$$

in which r_{FC} and L_{FC} are the resistance and inductance of the filter, while v_{DC} is the DC-link voltage.

B. Supercapacitors

The SC is represented by its well-known two-branch model [15], as shown in Fig. 1, in which C depends on its own voltage (u_{SC}) in accordance with

$$C = \sum_{k=0}^{1} c_k \, u_{SC}^k \tag{4}$$

where c_K are appropriate capacitive coefficients. In addition, the following relationships hold:

$$v_{SC} = r_d\, C_d \frac{d\,u_d}{dt} + u_d = r\, C \frac{d\,u_{SC}}{dt} + u_{SC} \tag{5}$$

$$-i_{SC} = C_d \frac{d\,u_d}{dt} + C \frac{d\,u_{SC}}{dt} \tag{6}$$

in which r, r_d, and C_d denote the parameters of the SC model shown in Fig. 1, while u_d and i_{SC} are auxiliary SC voltage and overall SC current respectively. The State-of-Energy (*SoE*) is computed as

$$SoE = \left(\frac{u_{SC}}{U_{SC}} \right)^2 \tag{7}$$

where U_{SC} denotes the SC rated voltage. Regarding the DC-DC converter and the SC inductive filter, (2) and (3) still apply but replacing the subscript FC with SC.

C. Batteries

The BP model derives from [16], [17] and leads to the following relationships:

$$v_{DC} = u_{BP} - r_{BP}\, i_{BP} + u_b \,, \quad -i_{BP} = \frac{u_b}{r_b} + C_b \frac{d\,u_b}{dt} \tag{8}$$

where u_{BP} and i_{BP} are the open-circuit voltage and BP current respectively, r_{BP} is the series resistance, u_b is the voltage across the RC branch, whose circuital parameters are denoted by r_b and C_b. Moreover, u_{BP} varies with the State-of-Charge (*SoC*) as

$$u_{BP} = u_{BP}^{(0)} - d \cdot (1 - SoC), \quad \frac{d\,SoC}{dt} = -\frac{i_{BP}}{Q_{BP}} \tag{9}$$

in which d is an appropriate coefficient and Q_{BP} is the BP rated capacity.

D. Other EPS components

ED and BK are modelled in a much less advanced fashion than FC, SC, and BP. In particular, ED is represented by its power exchange at the DC-link (p_{ED}), which is set in accordance with the traction effort required by the given driving cycle and which must satisfy the following constraint:

$$p_{ED} = v_{DC} \left(i_{FC}^{(DC)} + i_{SC}^{(DC)} + i_{BP} - i_{BK} \right) \tag{10}$$

in which i_{BK} is the rheostatic braking current that is modelled by an unconstrained current generator.

III. Energy Management System

A. Cost function and operating constraints

As in the previous competitions [13], [14], the aim of the EMS is minimizing the following cost function [12]:

$$\Phi = \Phi_{FC} + \Phi_{H_2} + \Phi_{SC} + \Phi_{BP} + \Phi_{ST} \tag{11}$$

in which each term is detailed in Table I, while the corresponding coefficients are reported in Table II. Particularly, Φ_{FC}, Φ_{SC} and Φ_{BP} account for FC, SC and BP degradation, while Φ_{H2} accounts for H_2 consumption. Furthermore, Φ_{ST} is the "charge sustaining cost", namely the cost needed for reinstating both *SoE* and *SoC* to their corresponding initial values at the end of the trip. Consequently, Φ_{ST} is the only term of Φ that can be negative, and it satisfies the following expression:

$$\Phi_{ST}\left(SoE^{(0)}, SoC^{(0)}\right) = 0\,. \tag{12}$$

Since the driving cycle is not known a priori, Φ minimization is hard to accomplish in real-time, as already pointed out in [10], [11]. Consequently, Φ minimization is addressed first by converting the global optimization problem into an instantaneous one by expressing Φ as

$$\Phi = \Phi_0 + \int_t \varphi d\tau\,, \quad \Phi_0 = c_{FC} n \Delta_{FC} \tag{13}$$

in which Φ_0 depends only on FC due to (12), while φ is

$$\varphi = \varphi_{FC} + \varphi_{BT} + \varphi_{SC} \tag{14}$$

where each term is detailed in Table III. In particular, φ_{FC} groups the integral term of both Φ_{FC} and Φ_{H2}, while φ_{SC} and φ_{BP} accounts for SC and BP degradation and charge sustaining costs introduced by Φ_{ST}. In this regard, the expressions of φ_{SC} and φ_{BP} reported in Table III are achieved by time-differentiating Φ_{ST} and then combining the results with (4)-(7) and (9), respectively. As a result, the minimization of Φ can be pursued by minimizing φ at every sampling time interval. However, the minimization of Φ and/or φ must be achieved by complying with (10) and all the other EPS constraints, which are summarized in Table IV. The latter reveals that FC and SC voltage and current constraints are set at component side, while (10) and BP constraints apply at the DC-link: this makes EPS constraint management not a trivial task, as detailed in the following subsection.

TABLE I Terms of the cost function

Term	Equation
Φ_{FC}	$c_{FC} n \Delta_{FC} + c_{FC} k_{FC} \int_0^t \left(1 + \alpha\left(1 - \frac{p_{FC}}{P_{FC}}\right)^2\right) d\tau$
Φ_{H2}	$c_{H_2} \int_0^t \frac{d m_{H_2}}{d\tau} d\tau$
Φ_{SC}	$c_{SC} k_{SC} \int_0^t 1\big\vert_{i_{SC}\neq 0}\, d\tau$
Φ_{BP}	$c_{BP} k_{BP} \int_0^t \left(1 + \frac{13}{4}(1-SoC)^2\right)\left(1 + \frac{\lvert i_{BP}\rvert}{2 I_{BP}} - \frac{i_{BP}}{20 I_{BP}}\right)\left\lvert\frac{i_{BP}}{I_{BP}}\right\rvert d\tau$
Φ_{ST}	$c_{H_2} \sum_{k=0}^{1} \left(g_k SoE^k + h_k SoC^k\right)$

B. Proposed MPC-based EMS

The overall scheme of the proposed MPC-based EMS is shown in Fig. 2. Starting from system inputs (Y), the first step consists of determining all the state variables X of the system (block A), most of which cannot be measured directly. In

TABLE II Main coefficients of the cost function

Symbol	Meaning	Value	Unit
c_{FC}	FC specific cost	1.2	k$
n	number of FC start & stop	-	-
Δ_{FC}	FC start-stop coefficient	$250\cdot10^{-6}$	-
k_{FC}	FC load coefficient	$13.9\cdot10^{-9}$	s^{-1}
α	FC load coefficient	4	-
P_{FC}	FC rated power	29.25	kW
c_{H2}	Hydrogen cost	$3.5\cdot10^{-3}$	$/g
c_{SC}	SC specific cost	2	k$
k_{SC}	SC load coefficient	$9.3\cdot10^{-9}$	s^{-1}
c_{BP}	BP specific cost	0.64	k$
k_{BP}	BP load coefficient	$18.5\cdot10^{-9}$	s^{-1}
I_{BP}	BP base current	262.8	kA

TABLE III Terms of the integral cost function

Term	Equation
φ_{FC}	$c_{FC} k_{FC}\left(1 + \alpha\left(1 - \frac{p_{FC}}{P_{FC}}\right)^2\right) + c_{H_2} \sum_{k=0}^{1} b_k i_{FC}^k$
φ_{SC}	$c_{SC}\big\vert_{i_{SC}\neq 0} - 2 c_{H_2} g_1 \frac{u_{SC}}{U_{SC}^2} \frac{r_d i_{SC} + u_{SC} - u_d}{(r + r_d) C}$
φ_{BP}	$c_{BP} k_{BP}\left(1 + \frac{13}{4}(1-SoC)^2\right)\left(1 + \frac{\lvert i_{BP}\rvert}{2 I_{BP}} - \frac{i_{BP}}{20 I_{BP}}\right)\lvert i_{BP}\rvert - c_{H_2} h_1 \frac{i_{BP}}{Q_{BP}}$

TABLE IV Operating constraints

Component	Variable	Min	Max
FC	i_{FC}	-	$\overline{I}_{FC}$
	di_{FC}/dt	$-\Delta\overline{I}_{FC}$	$\Delta\overline{I}_{FC}$
	p_{FC}	-	$\overline{P}_{FC}$
SC	SoE	$\underline{e}_{SC}$	$\overline{e}_{SC}$
	v_{SC}	-	$\overline{V}_{SC}$
	p_{SC}	-	$\overline{P}_{SC}$
BP	SoC	$\underline{e}_{BP}$	$\overline{e}_{BP}$
	i_{BP}	$-\overline{I}_{BP}$	$\overline{I}_{BP}$
	v_{DC}	$\underline{V}_{DC}$	$\overline{V}_{DC}$

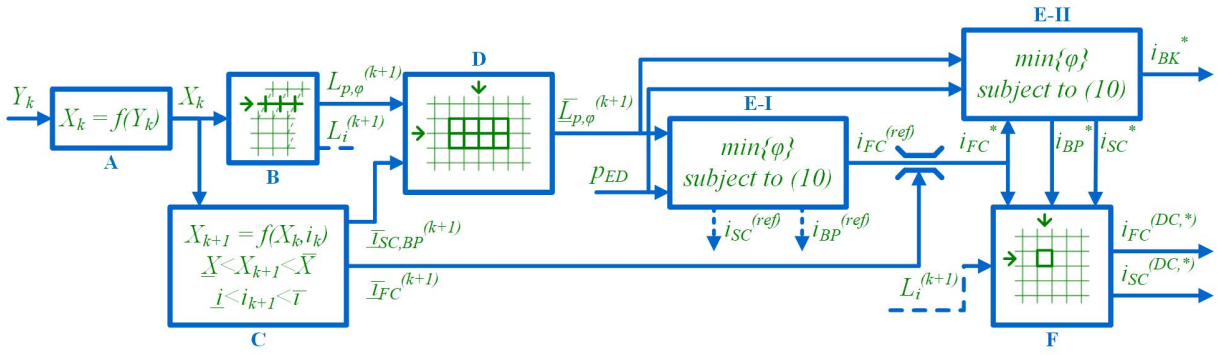

Fig. 2. The schematic view of the proposed MPC-based EMS: A) state variable computation; B) look-up table selection; C) MPC-based constraint management; D) look-up table refinement; E-I,E-II) optimization; F) DC-link reference current selection.

TABLE V LUT DEPENDENCY

LUT(s)	State variable(s)	Current(s)
$p_{FC}^{(DC)}, i_{FC}^{(DC)}$	$u_{BP} + u_b$	i_{FC}, i_{BP}
φ_{FC}	-	i_{FC}
$p_{SC}^{(DC)}, i_{SC}^{(DC)}$	u_{SC}, u_d, $u_{BP} + u_b$	i_{SC}, i_{BP}
φ_{SC}	u_{SC}, u_d	i_{SC}
p_{BP}	$u_{BP} + u_b$	i_{BP}
φ_{BP}	SoC	i_{BP}

particular, starting from SoE, u_{SC} is computed easily by (7). Then, u_{SC}, v_{SC} and i_{SC} concur to determine u_d through (5)-(6). Similar considerations apply to BP, namely u_{BP} is computed in accordance with (9), while u_b is determined based on u_{BP}, i_{BP} and v_{DC} by means of (8).

Once all state variables at the k-th sampling time instant have been calculated, the most appropriate Look-Up Tables (LUTs) have to be selected; these stores the values of DC-link powers, currents and cost functions for each component (FC, SC and BP) as a function of their corresponding currents and of some state variables, as pointed out in Table V. Particularly, this reveals a strong coupling between BP and both FC and SC because any variation of i_{BP} results in a variation of v_{DC} and, thus, of both current and voltage values of FC and SC. It is worth highlighting that all LUTs have been determined offline at steady-state operation, by varying state variables and currents within appropriate ranges. Consequently, LUTs do not account for L_{FC} and L_{SC}, also because their values are rather negligible in terms of power exchanged at the DC-link. Therefore, assuming that the state variables slowly vary within the chosen sampling time interval (T_s), it is possible to extract suitable sub-LUTs that depend on FC, SC and BP currents only ($L_p^{(k+1)}$, $L_i^{(k+1)}$, $L_\varphi^{(k+1)}$), as shown in Fig. 2 (block B).

In order to make $L_p^{(k+1)}$ and $L_\varphi^{(k+1)}$ compliant with the operating constraints reported in Table IV, an MPC approach characterized by a control horizon of one sampling time is followed. Considering FC at first, the relationships among FC current, voltage and power are analytical, as highlighted by (1)-(2). Therefore, all FC constraints can be converted into corresponding equivalent FC current constraints easily, leading to determine maximum and minimum i_{FC} values ($\underline{I}_{FC}^{(k+1)}$). Different considerations apply to SC, namely (5)-(6) needs to be converted into their corresponding sample-data versions as

$$\begin{aligned} x_{SC}^{(k+1)} &= F_{SC}\, x_{SC}^{(k)} + H_{SC}\, i_{SC}^{(k)} \\ v_{SC}^{(k+1)} &= C_{SC} x_{SC}^{(k)} + d_{SC}\, i_{SC}^{(k)} \end{aligned} \tag{15}$$

in which x_{SC} denotes $[u_{SC}, u_d]$, while F_{SC}, H_{SC}, C_{SC} and d_{SC} depend on SC coefficients and T_s in accordance with (5)-(6). Therefore, based on (7) and (15), all SC constraints can be converted into equivalent SC current constraints by computing $\underline{I}_{SC}^{(k+1)}$. The same approach is followed for BP, namely (8)-(9) leads to

$$\begin{aligned} x_{BP}^{(k+1)} &= F_{BP}\, x_{BP}^{(k)} + H_{BP}\, i_{BP}^{(k)} \\ v_{DC}^{(k+1)} &= v_{DC}^{(0)} + C_{BP} x_{BP}^{(k)} + d_{BP}\, i_{BP}^{(k)} \end{aligned} \tag{16}$$

in which $x_{BP} = [u_b, SoC]$, while F_{BP}, H_{BP}, $v_{DC}^{(0)}$, C_{BP} and d_{BP} depend on BP coefficients and T_s in accordance with (8)-(9). As a result, all BP constraints can be converted into equivalent BP current constraints, enabling the identification of $\underline{I}_{BP}^{(k+1)}$.

Once maximum and minimum current values have been determined (block C), $\underline{L}_p^{(k+1)}$ and $\underline{L}_\varphi^{(k+1)}$ can be extracted suitably from $L_p^{(k+1)}$ and $L_\varphi^{(k+1)}$ by considering just the allowable ranges of both i_{SC} and i_{BP} (block D). It is worth noting that the same is not done with i_{FC} because the strict constraint imposed on its time derivative could force the system to operate in a local optimum. Consequently, FC current constraints are ignored at the first stage of the optimization (block E-I): particularly, $\underline{L}_p^{(k+1)}$ are combined all together ($\mathcal{L}_p^{(k+1)}$) and the same is carried out for $\underline{L}_\varphi^{(k+1)}$ ($\mathcal{L}_\varphi^{(k+1)}$). After this, all the $\mathcal{L}_p^{(k+1)}$ values smaller than p_{ED} are disregarded, as well as the corresponding $\mathcal{L}_\varphi^{(k+1)}$ values; this is because i_{BK} (p_{BK}) is always positive, meaning that the available power at the DC-link has to be greater than or at least equal to p_{ED}. As a result, the first stage of optimization can be accomplished by identifying the i_{FC}, i_{BP} and i_{SC} indexes corresponding to the minimum φ value among the remaining elements of $\mathcal{L}_\varphi^{(k+1)}$. However, the only outcome needed for carrying on the optimization procedure is $i_{FC}^{(ref)}$, so all the others are disregarded.

Given $i_{FC}^{(ref)}$, it is properly bounded in accordance with $\underline{I}_{FC}^{(k+1)}$ previously determined (block C). The corresponding result (i_{FC}^*) is employed for carrying out the second stage of optimization (block E-II), which also requires $\underline{L}_p^{(k+1)}$, $\underline{L}_\varphi^{(k+1)}$ and p_{ED}. Apart from i_{FC}^*, which is not optimized further, the same procedure followed at the first stage applies, yielding i_{BP}^*, i_{SC}^*,

and i_{BK}^*. Both i_{FC}^* and i_{SC}^* are further processed (block F), together with i_{BP}^*, in order to achieve the corresponding reference currents at the DC-link by means of $L_i^{(k+1)}$ previously computed (block B). On th other hand, outputting i_{BP}^* is not needed due to the passive connection of BP to the DC-link.

IV. Simulation Results

The proposed MPC-based EMS is tested through numerical simulations, which are carried out in MATLAB-Simulink by employing the files made available by the competition [12]. In this regard, component models and local control systems run at fixed-step (T_{sim} = 1 ms), while T_s has been set to 500 ms in order to achieve a suitable trade-off between control accuracy and overall simulation time. Furthermore, a default EMS was already available, which has been considered for comparison purposes. This consists of a simple rule-based approach (RB-EMS), in which FC is activated only when the *SoE* drops below a given threshold (0.8): in those cases, FC reference current is set at the sum between i_{ED} and 5 A in order to recharge SC suitably. This FC reference current value is then processed further in order to comply with the FC current constraints reported in Table IV. Instead, the SC reference current is set at the difference between i_{ED} and i_{FC} multiplied by a scaling factor (0.95) in order to enable SC to share part of the power with BP.

Simulation results are shown from Fig. 3 to Fig. 5, which refer to a short real driving cycle of about 3 min (S-DC), and in Table VI, which also accounts for much longer driving cycles (NEDC - 13 min, L-DC - 20 min). Focusing on S-DC at first, it can be seen that the overall cost is due almost exclusively to FC degradation and, to a less extent, to H_2 consumption, especially in the case of RB-EMS. In this regard, the proposed MPC-based EMS is able to minimize FC turns on/off compared to RB-EMS, resulting in a much lower FC degradation. Reduced FC degradation achieved by MPC-based EMS is due also to maintaining FC power at an almost constant rate, while BP (SC) is exploited much more (less) than RB-EMS; this seemingly

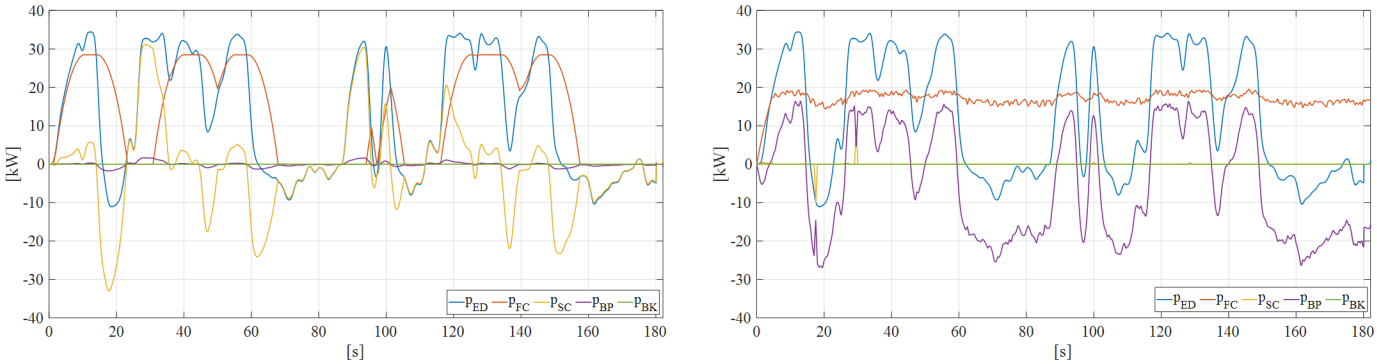

Fig. 3. Powers achieved by employing the RB-EMS (on the left) and the proposed MPC-based EMS (on the right).

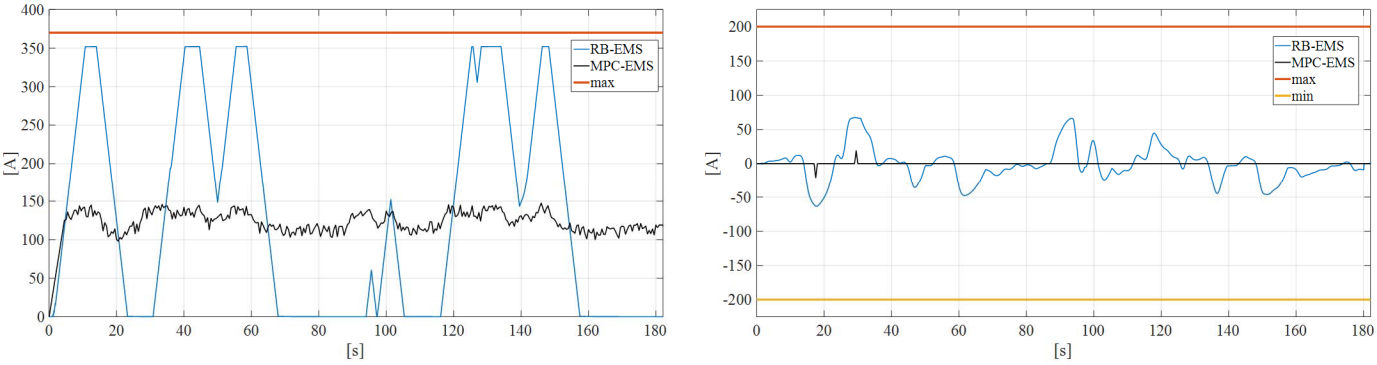

Fig. 4. FC and SC currents (left and right respectively) achieved by employing the RB-EMS and the proposed MPC-based EMS.

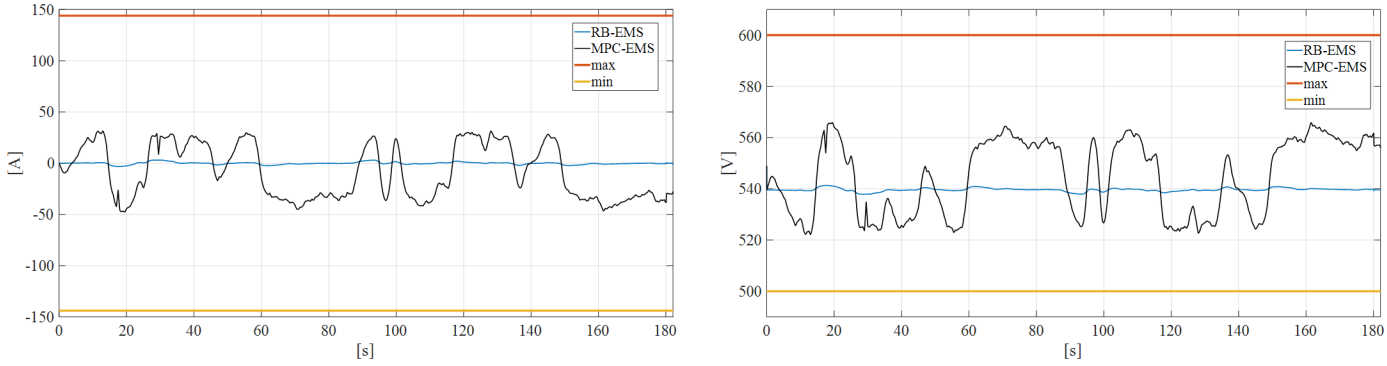

Fig. 5. BP currents and DC-link voltages (left and right respectively) achieved by employing the RB-EMS and the proposed MPC-based EMS.

TABLE VI COST FUNCTION VALUES (IN C$)

Term	EMS	S-DC	NEDC	L-DC
Φ_{FC}	RB-EMS	210.480	781.480	3664.930
	MPC-EMS	30.520	32.308	33.380
Φ_{H2}	RB-EMS	12.699	22.094	91.376
	MPC-EMS	12.755	53.764	85.528
Φ_{BP}	RB-EMS	0.000	0.000	0.000
	MPC-EMS	0.000	0.000	0.000
Φ_{SC}	RB-EMS	0.331	1.032	2.0886
	MPC-EMS	0.004	0.256	0.107
Φ_{ST}	RB-EMS	–0.786	–0.716	0.157
	MPC-EMS	–3.644	–35.785	–17.386
Φ	RB-EMS	222.720	803.890	3758.550
	MPC-EMS	39.635	20.544	101.630

anomalous exploitation is due to degradation costs, which are much lower for BP than for SC, as proved by the zero-value achieved for BP over any driving cycle (Table VI). Consequently, MPC-based EMS forces BP to act as an energy buffer, while SC is rarely employed, just when high power peaks occur. Moreover, MPC-based EMS charged BP over S-DC in order to optimize Φ_{ST} properly. As a result, further cost reductions are achieved, as pointed out in Table VI.

Similar considerations apply to both NEDC and L-DC, as still pointed out in Table VI. In particular, apart from reducing FC degradation compared to RB-EMS, MPC-based EMS increases H_2 consumption over NEDC in order to recharge BP suitably, leading to a further cost reduction. SC degradation is reduced as well, by exploiting the very low BP degradation costs and, thus, prioritizing the use of BP instead of SC; this has been enabled by MPC-EMS through an appropriate management of all operating constraints, which is mandatory because i_{BP} significantly affects DC-link voltage evolution, as highlighted in Fig. 5. Consequently, since v_{DC} fluctuations affect both i_{FC} and i_{SC}, some operating constraints could be violated easily unless accurate modelling and management are not employed. The results thus reveal the effectiveness of the proposed MPC-based EMS over different operating conditions.

V. CONCLUSION

An Energy Management System (EMS) based on a Model Predictive Control (MPC) approach has been presented in this paper, which aims at minimizing the operating costs of a Hybrid Electric Vehicle (HEV). The proposed EMS is able to identify the allowable ranges of each HEV control variable at every sampling time interval, within which the optimal solution is selected through suitable look-up tables. Simulation results reveal the superior performance achieved by the proposed MPC-based EMS compared to a basic rule-based EMS, especially in terms of reduced fuel cell and supercapacitor degradation, as well as charge sustaining costs. This comes at the cost of using battery much more than expected, which may cause its unsuitable lifetime reduction. However, this issue can be solved easily by increasing battery degradation cost accordingly, without affecting the validity of the proposed MPC-based EMS.

REFERENCES

[1] M. Ehsani, Y. Gao, and A. Emadi, *Modern Electric, Hybrid Electric, and Fuel Cell Vehicles: Fundamentals, Theory, and Design, Second Edition*. CRC Press, 2009.

[2] N. Sulaiman, M. A. Hannan, A. Mohamed, E. H. Majlan, and W. R. Wan Daud, "A review on energy management system for fuel cell hybrid electric vehicle: Issues and challenges," *Renew. Sustain. Energy Rev.*, vol. 52, pp. 802–814, Dec. 2015, doi: 10.1016/j.rser.2015.07.132.

[3] A. Tani, M. B. Camara, and B. Dakyo, "Energy Management Based on Frequency Approach for Hybrid Electric Vehicle Applications: Fuel-Cell/Lithium-Battery and Ultracapacitors," *IEEE Trans. Veh. Technol.*, vol. 61, no. 8, pp. 3375–3386, Oct. 2012, doi: 10.1109/TVT.2012.2206415.

[4] M. Porru, A. Serpi, A. Salimbeni, and A. Damiano, "An advanced frequency-based energy management of hybrid energy storage systems for microgrids," in *IECON 2017 - 43rd Annual Conference of the IEEE Industrial Electronics Society*, 2017, pp. 7617–7622, doi: 10.1109/IECON.2017.8217335.

[5] X. Li, J. Li, L. Xu, and M. Ouyang, "Power management and economic estimation of fuel cell hybrid vehicle using fuzzy logic," in *Proc. of 5th IEEE Vehicle Power and Propulsion Conference (VPPC 2009)*, Dearborn (USA), 2009, pp. 1749–1754, doi: 10.1109/VPPC.2009.5289696.

[6] C. Weyers and T. Bocklisch, "Simulation-based investigation of energy management concepts for fuel cell – battery – hybrid energy storage systems in mobile applications," *Energy Procedia*, vol. 155, pp. 295–308, Nov. 2018, doi: 10.1016/j.egypro.2018.11.048.

[7] A. Serpi, M. Porru, and A. Damiano, "An Optimal Power and Energy Management by Hybrid Energy Storage Systems in Microgrids," *Energies*, vol. 10, no. 11, p. 1909, Nov. 2017, doi: 10.3390/en10111909.

[8] H. Jiang, L. Xu, J. Li, Z. Hu, and M. Ouyang, "Energy management and component sizing for a fuel cell/battery/supercapacitor hybrid powertrain based on two-dimensional optimization algorithms," *Energy*, vol. 177, pp. 386–396, Jun. 2019, doi: 10.1016/j.energy.2019.04.110.

[9] H. Li, A. Ravey, A. N'Diaye, and A. Djerdir, "Equivalent consumption minimization strategy for hybrid electric vehicle powered by fuel cell, battery and supercapacitor," in *Proc. of 42nd Annual Conference of the IEEE Industrial Electronics Society (IECON 2016)*, Florence (Italy), 2016, pp. 4401–4406, doi: 10.1109/IECON.2016.7794047.

[10] A. Serpi and M. Porru, "Modelling and Design of Real-Time Energy Management Systems for Fuel Cell/Battery Electric Vehicles," *Energies*, vol. 12, no. 22, p. 4260, Jan. 2019, doi: 10.3390/en12224260.

[11] A. Serpi and M. Porru, "A Multi-Stage Energy Management System for Multi-Source Hybrid Electric Vehicles," in *IECON 2019 - 45th Annual Conference of the IEEE Industrial Electronics Society*, 2019, vol. 1, pp. 5901–5908, doi: 10.1109/IECON.2019.8926840.

[12] J. Solano, S. Jemei, L. Boulon, L. Silva, D. Hissel, and M.-C. Pera, "IEEE VTS Motor Vehicles Challenge 2020 - Energy Management of a Fuel Cell/Ultracapacitor/Lead-Acid Battery Hybrid Electric Vehicle," in *2019 IEEE Vehicle Power and Propulsion Conference (VPPC)*, 2019, pp. 1–6, doi: 10.1109/VPPC46532.2019.8952246.

[13] C. Depature *et al.*, "IEEE VTS Motor Vehicles Challenge 2017 - Energy Management of a Fuel Cell/Battery Vehicle," in *2016 IEEE Vehicle Power and Propulsion Conference (VPPC)*, 2016, pp. 1–6, doi: 10.1109/VPPC.2016.7791701.

[14] W. Lhomme *et al.*, "IEEE VTS Motor Vehicles Challenge 2019 - Energy Management of a Dual-Mode Locomotive," in *2018 IEEE Vehicle Power and Propulsion Conference (VPPC)*, 2018, pp. 1–6, doi: 10.1109/VPPC.2018.8605044.

[15] L. Zubieta and R. Bonert, "Characterization of double-layer capacitors for power electronics applications," *IEEE Trans. Ind. Appl.*, vol. 36, no. 1, pp. 199–205, Jan. 2000, doi: 10.1109/28.821816.

[16] M. Ceraolo, "New dynamical models of lead-acid batteries," *IEEE Trans. Power Syst.*, vol. 15, no. 4, pp. 1184–1190, Nov. 2000, doi: 10.1109/59.898088.

[17] K. El Kadri and A. Berthon, "Energy Management Operating Modes Concerning a Hybrid Heavy Vehicle," in *EUROCON 2007 - The International Conference on "Computer as a Tool,"* 2007, pp. 1587–1593, doi: 10.1109/EURCON.2007.4400566.